Journal of Materials Chemistry A

Interface-induced Crystallization and Nanostructure Formation of [6,6]-Phenyl-C_{61}-butyric Acid Methyl Ester (PCBM) in Polymer Blend Films and Its Application in Photovoltaics

Journal:	*Journal of Materials Chemistry A*
Manuscript ID	TA-ART-11-2015-009545.R1
Article Type:	Paper
Date Submitted by the Author:	21-Jan-2016

Complete List of Authors:	Zhong, Yufei; RIKEN Center for Emergent Matter Science (CEMS), Supramolecular Chemistry Division Suzuki, Kaori; RIKEN Center for Emergent Matter Science (CEMS), Supramolecular Chemistry Division Inoue, Daishi; RIKEN, Materials Characterization Support Unit hashizume, Daisuke; Riken, Izawa, Seiichiro; RIKEN Center for Emergent Matter Science (CEMS), Supramolecular Chemistry Division Hashimoto, Kazuhito; The University of Tokyo, Research Centre for Advanced Science and Technology Koganezawa, Tomoyuki; SPring-8 Tajima, Keisuke; RIKEN Center for Emergent Matter Science (CEMS), Supramolecular Chemistry Division

Interface-induced Crystallization and Nanostructure Formation of [6,6]-Phenyl-C_{61}-butyric Acid Methyl Ester (PCBM) in Polymer Blend Films and Its Application in Photovoltaics

Yufei Zhong[1,2¶], *Kaori Suzuki*[2], *Daishi Inoue*[2], *Daisuke Hashizume*[2], *Seiichiro Izawa*[1,2], *Kazuhito Hashimoto*[1], *Tomoyuki Koganezawa*[3] *and Keisuke Tajima*[2,4*]

[1]Department of Applied Chemistry, School of Engineering, The University of Tokyo, 7-3-1 Hongo, Bunkyo-ku, Tokyo 113-8656, Japan, [2]RIKEN Center for Emergent Matter Science (CEMS), 2-1 Hirosawa, Wako 351-0198, Japan, [3]Japan Synchrotron Radiation Research Institute, 1-1-1 Kouto, Sayo-cho, Sayo-gun, Hyogo 679-5198, Japan, and [4]Japan Science and Technology Agency, PRESTO, 4-1-8 Honcho Kawaguchi, Saitama 332-0012, Japan

[¶] Current address: Materials Science and Engineering, Physical Sciences and Engineering Division, King Abdullah University of Science and Technology (KAUST), Thuwal 23955-6900, Saudi Arabia.

Abstract

Crystallization of [6,6]-phenyl-C_{61}-butyric acid methyl ester (PCBM) in thin films and in blend films with various polymers was investigated by X-ray diffraction.

Thermal annealing induced the crystallization of PCBM in the blend films only through direct contact with a crystallized pure PCBM layer beneath, suggesting epitaxial crystallite growth occurred from the bottom interface. The morphology of the crystals depended strongly on the mixing ratio and the crystal structure of the bottom layer, and nanorod-like PCBM crystallites with widths of 100–150 nm and lengths of 150–500 nm were observed. Bulk-heterojunction (BHJ) organic solar cell utilizing the PCBM crystallite as the acceptor showed the highest V_{OC} of 0.83 V for PTB7:PCBM device to date. These findings offer the ways to use the crystallized PCBM with the controlled nanostructures as the electron conducting materials in organic and hybrid perovskite photovoltaics.

Introduction

Crystallization of organic semiconductors plays an essential role in determining the performance of electronic devices such as field effect transistors and organic solar cells (OSCs).[1, 2] In solution-processed organic semiconductor films, crystallization often occurs during the coating processes; thus, the coating conditions, such as the solvent and temperature, can be tuned to control nucleation and crystal growth. Precise control of the conditions can produce large oriented single-crystal films.[3] Alternatively, the materials can be crystallized by post-treatment starting from amorphous films, where random nucleation triggers the formation of multi-crystalline domains that significantly improve the connectivity of carrier pathways in the film.[4] However, mixed films that contain two semiconducting materials have mixed bulk heterojunctions (BHJ) and are often used for OSCs. In these films, the crystallization of each material is much more complicated and hard to control because the crystallinity and sizes of the phase-separated domains and the connectivity of each material are important for the performance.[5]

[6,6]-Phenyl-C_{61}-butyric acid methyl ester (PCBM) is the most widely used electron acceptor material in OSCs. Unlike C_{60}, PCBM shows low crystallinity owing to its low structural symmetry. The single-crystal structure of PCBM without incorporated solvent molecules was reported only recently.[6,7] The thermally induced crystallization of pure PCBM in thin films was first reported by Bao et al.[8] Recently, we investigated the effects of the crystallization on the electronic energy levels of pure PCBM films.[9]

We observed that the crystallized PCBM films exhibited smaller electron affinity (EA) than that of amorphous PCBM. This is of particular interest for OSC since EA of the acceptor materials determine the highest V_{OC} attainable in OSCs. In addition, a lot of recent research show that there is a strong relationship between the molecular order and high charge separation efficiency in OSCs.[10, 11] Highly crystalline materials may increase the charge separation efficiency either through more delocalized charge transfer states at the interface[10, 12] or cascade charge transfer induced by proper energy level alignment.[11, 13-16] Consequently, use of the crystallized PCBM in BHJ structures could potentially lead to further improvement of the performance in OSCs[17].

Nevertheless, the control of the aggregation or the crystallization behaviors of PCBM in BHJ blend films remains challenging. Much effort has focused on optimizing the mixed morphology in BHJ by post-treatment of the mixed films such as thermal annealing, exposure to solvent vapors, or by using additives in the coating solutions.[1, 18, 19] In high-performance OSCs, however, the crystallization of PCBM in BHJ films has not been observed. X-ray diffraction (XRD) of the BHJ films generally shows only a broad halo from PCBM; therefore, it is thought that PCBM simply aggregates and forms a pure phase separated from the donor materials.[20] PCBM can be crystallized in BHJ films only by long, harsh thermal annealing, typically above the glass transition temperature of the polymers. However, the crystals grow to a macroscopic size (5–50μm) and the performance of OSCs deteriorates significantly owing to the decrease in the area of interfaces between the materials.[21-23] Crystallizing

PCBM with much smaller size in BHJs, ideally comparable to the exciton diffusion length (~20 nm), could be advantageous for OSCs. Although there are several approaches to controlling the macroscopic crystallization of PCBM, for example, by using additives in the solutions or in cross-linking the components,[24, 25] or by using mica substrates to regulate the shape of the crystals on the micrometer scale,[26] the control of the nucleation and crystal growth of PCBM to form nanoscale crystallites have never been reported.

In this study, we discovered a novel interface-induced crystallization of PCBM in blend films consisting of various polymers. In this approach, a pure thermally crystallized PCBM film was used as a seed layer and the blend films of polymer and PCBM were transferred onto the seed layer.[27, 28] After subsequent thermal annealing, epitaxial growth of PCBM crystallites occurred from the bottom interface as shown schematically in Figure 1. The polymers poly({4,8-bis[(2-ethylhexyl)oxy]benzo[1,2-b:4,5-b']dithiophene-2,6-diyl}{3-fluoro-2-[(2-ethylhexyl)carbonyl]thieno[3,4-b]thiophenediyl}) (PTB7), poly(3-hexylthiophene) (P3HT), and polystyrene (PS) were used to demonstrate the wide applicability of this methodology (Figure 1). Grazing incidence X-ray diffraction (GIXRD) and scanning electron microscopy (SEM) were used to characterize PCBM crystallization in the blend films. OSCs with BHJ structure using the crystallized PCBM as the electron acceptor was demonstrated for the first time.

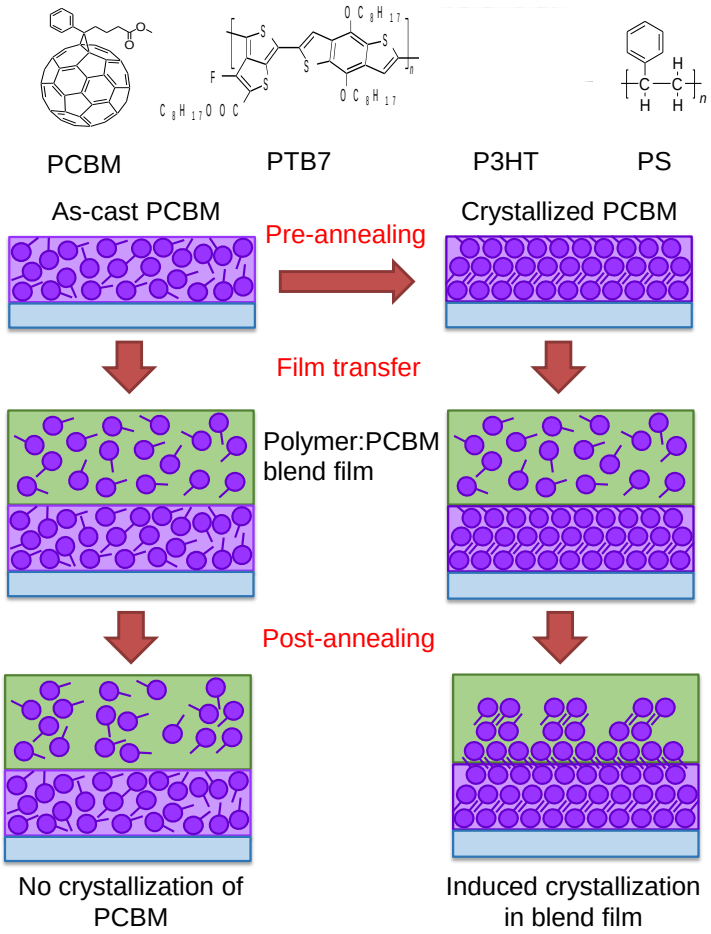

Figure 1. Chemical structures of the materials used in this study and schematic illustration of induced crystallization of PCBM in blend films. The crystallized PCBM film is obtained by pre-annealing of the as-cast amorphous film and used as the seed layer. A mixed film of PCBM and a polymer is transferred onto the crystallized PCBM film. After post-annealing, the amorphous PCBM in the bulk heterojunction layer crystallizes from the bottom interface. When the as-cast PCBM film is used as the seed layer, no crystallization of PCBM is induced.

Results and discussion

The in-plane GIXRD pattern of as-cast pure PCBM films with a thickness of 40 nm showed a broad peak at 19.5° (Figure 2a), indicating an amorphous structure. After

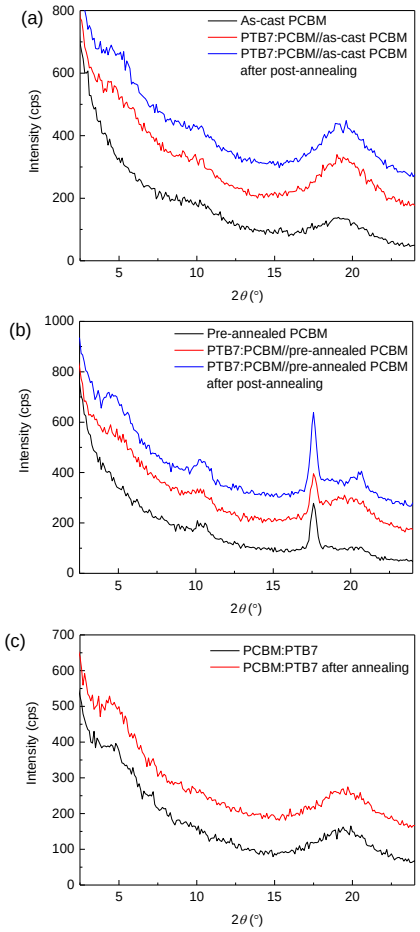

Figure 2. In-plane GIXRD patterns of (a) as-cast PCBM films (black) and PTB7:PCBM//as-cast PCBM films before (red) and after post-annealing (blue), (b) pre-annealed PCBM film (black) and PTB7:PCBM//pre-annealed PCBM films before (red) and after post-annealing (blue), and (c) spin-coated PTB7:PCBM films before (black) and after annealing (red). The patterns are shifted in the *y*-axis for clarity.

annealing at 150°C for 5 min, a sharp peak appeared at 17.5° and broader and smaller peaks appeared at 10.8° and 20.5°, while the broad peak at 19.5° decreased, suggesting that PCBM crystallized (Figure 2b). This is consistent with previous reports[9] and it happens independently on the film substrates (Figure S1 in Supporting Information (SI)). We call this process "pre-annealing" in this paper, and the pure PCBM films with and without pre-annealing were used as the seed layer in the following experiments (Figure 1).

A mixed BHJ layer of PTB7:PCBM spin-coated on the TiO_2/ITO substrates did not show any crystallization of PCBM upon thermal annealing under the same conditions (150°C for 5 min, Figure 2c). Only a slight increase in the peak intensity at 5° was observed, which can be attributed to the development of the face-on lamellar structure of PTB7.[29] No change was observed in the halo at 19.5° upon heating, indicating that PCBM did not crystallize in the BHJ layer during annealing, although the aggregation state could be changed. The same result was obtained when the mixed BHJ layer was transferred onto the as-cast PCBM film without pre-annealing, by using the film transfer method. This sample is referred to as the PTB7:PCBM//as-cast PCBM film, where the layers are written from top to bottom and // denotes the transferred interface. As shown in Figure 2a, PTB7:PCBM//as-cast PCBM film showed a more intense amorphous halo at 19.5° from PCBM in the top BHJ layer. There was no change in the halo observed after post-annealing of this sample at 150°C for 5 min. This indicates that the interface of the as-cast amorphous PCBM did not induce

crystallization of PCBM in the BHJ layer.

BHJ films were transferred onto the pre-annealed, crystallized PCBM films (PTB7:PCBM//pre-annealed PCBM) in a similar manner. After the film transfer, the broad peak at 19.5° appeared again owing to the amorphous PCBM in the top BHJ layer (Figure 2b). The intensity of the peaks from the crystallized PCBM remained the same because the transfer process does not change the structure of the bottom layer and the incident angle for the GIXRD measurement (0.21°) is large enough to detect the entire films. In contrast to the PTB7:PCBM//as-cast PCBM film, after post-annealing of the film at 150 °C for 5 min, the intensity of the peaks from crystallized PCBM (17.5°, 10.8° and 20.5°) increased, while the halo at 19.5° decreased. These results indicate that the amorphous PCBM in the BHJ layer crystallized after post-annealing only in the presence of the crystallized PCBM layer at the bottom. This strongly suggests that the crystallization occurred from the crystallized PCBM interface, possibly via epitaxial growth.

Atomic force microscopy and optical microscopy on PTB7:PCBM//pre-annealed PCBM before and after post-annealing show small changes in the surface roughness and no macroscopic crystallization occurred in the films (Figures S2 and S3). This indicates that the crystallization of PCBM in PTB7:PCBM observed here is different from the macroscopic phase separation often observed for OSCs when mixed films are annealed for a long time.[21-23]

Dependence of the crystallization behavior on the thickness of PTB7:PCBM layer

was also investigated. As shown in Figure S4, the same changes were observed for the thicker BHJ films up to 235 nm after post-annealing: the sharp peaks from PCBM crystals increased, the intensity of the lamellar peak from PTB7 increased, and the halo from the amorphous PCBM in PTB7:PCBM layer decreased. When the thicker BHJ layer was used, the peak intensities increased, suggesting that the amount of the crystallized PCBM in BHJ increased with the film thickness. This could imply that the induced crystallization of PCBM happened in the region near the interface and also propagated to the bulk of the BHJ layer. The time and temperature for post-annealing were also varied from 5 to 15 min and from 150 to 180 °C, respectively (Figure S5). The results show that after post-annealing at 150 °C for 5 min the crystallization of PCBM in PTB7:PCBM layer reached its limit and the diffraction did not change further when the thickness was up to 132 nm. As the thickness of the PCBM:PTB7 layer increased, a longer time was needed to complete the crystallization of PCBM. For example, more than 20 min was required for the 235-nm-thick layer to crystallize (Figure S6). This result suggested that the diffusion of PCBM in the PTB7:PCBM layer limits the rate of crystallization.

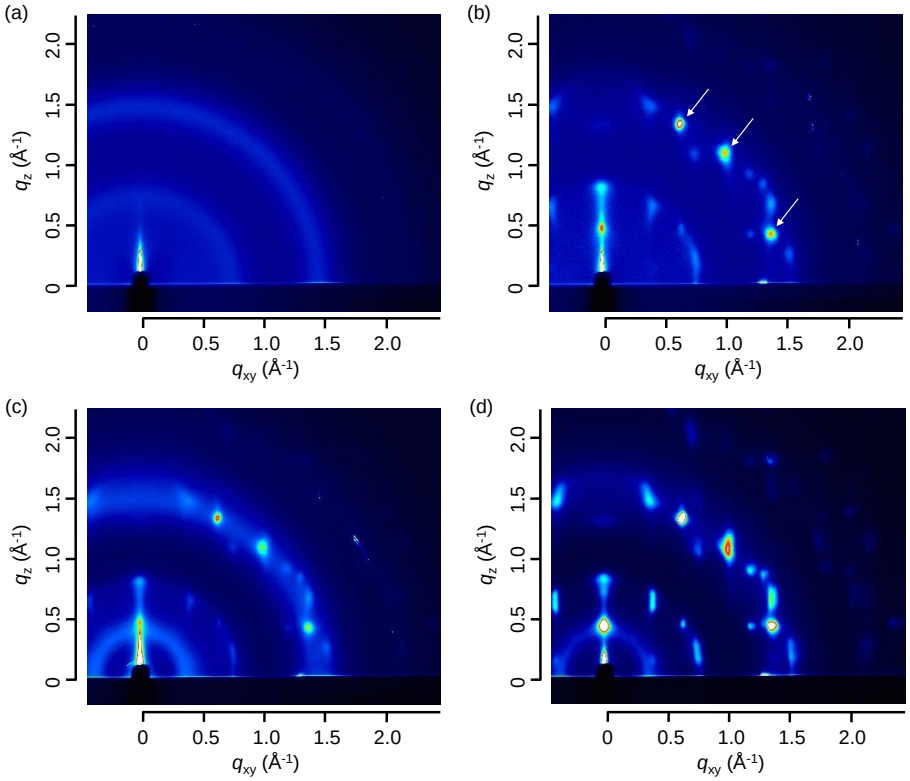

Figure 3. 2D GIXRD measurements of (a) as-cast PCBM, (b) pre-annealed PCBM, (c) PTB7:PCBM//pre-annealed PCBM, and (d) PTB7:PCBM//pre-annealed PCBM films after post-annealing. The arrowed peaks in (b) are mentioned in the main text.

2D GIXRD measurements of the films were performed with synchrotron radiation (Figure 3). The as-cast PCBM film showed broad rings at q of 0.75 and 1.48 Å^{-1} (Figure 3a), indicating an isotropic amorphous structure. After pre-annealing, the PCBM film showed a punctiform diffraction pattern with particularly intense spots at q of 1.38, 1.39, and 1.37Å^{-1} (arrowed peaks in Figure 3b). The appearance of the multiple spots with the same q suggests that there are several preferred orientations of PCBM crystal domains in the films. The peaks at q_{xy} of 0.74 Å^{-1}, 1.25 Å^{-1}, and 1.45 Å^{-1} are consistent with the in-plane GIXRD patterns. This is also consistent with

selected area electron diffraction (SAED) of the film observed during transmission electron microscopy (Figure S7). The SAED pattern shows a strong single spot with q of 1.26 $Å^{-1}$, suggesting that the lateral domain size of the crystallite is larger than the selected area (φ = 230 nm). After the transfer of the PTB7:PCBM layer onto the crystallized PCBM layer, a broad ring at q = 0.4 $Å^{-1}$ appeared, which originated from the lamellar structure of PTB7 (Figure 3c). In addition, the broad rings from amorphous PCBM appeared again because aggregated PCBM was present in the PTB7:PCBM layer. After post-annealing, the intensity of the amorphous PCBM rings decreased and the diffraction spots from the PCBM crystal intensified and broadened slightly, although no new spots appeared (Figure 3d). This result indicates that PCBM in the PTB7:PCBM layer crystallized after post-annealing with a crystal structure and orientation similar to those of the bottom PCBM layer.

To gain better understanding of the crystal structure in the films, we first analyzed the powder diffraction pattern of PCBM by using the single-crystal structure reported by Casalegno et al. to assign the peaks in XRD patterns.[7] The simulated pattern reproduced the experimental data well with slightly different lattice parameters (Figure S8 and Table S1). By assuming the same crystal structure in the films, we tried to assign the peaks in the in-plane patterns and 2DGIXRD data of PCBM films. However, the diffraction patterns could not be reproduced, even with slightly distorted lattice parameters. This result suggests that the crystal structure in the annealed film is different from the single-crystal structure and the powder sample.

Taking the successful nanoscale crystallization of PCBM in the mixed BHJ, we fabricated OSCs by depositing MoO_3/Ag on the film surface (ITO/TiO_2/active layer/ MoO_3/Ag). The BHJ layers were either directly spin coated on TiO_2/ITO or transferred onto the PCBM seed layers. The PCBM seed layers were either as-cast (amorphous) or pre-annealed (crystallized). Then the active layers were either used as cast (no crystallization in BHJ) or annealed at 150 °C for 5 min prior to the deposition of MoO_3/Ag (crystallization in BHJ when the crystallized seed layer is underneath). The performances of the six OSCs with the different fabrication conditions are summarized in Table 1 (typical *J*-*V* curves in Figure S15). Note that we did not use 1,8-diiodooctane (DIO) as the solvent additive to optimize the blend morphology of PTB7:PCBM, so the performance was lower than those of the optimized cells. Here we try to observe the effect of the PCBM crystallization in BHJ rather than to achieve high performance. We observed similar V_{OC} of ~0.75 V in all the cases except PTB7:PCBM//pre-annealed PCBM device with post-annealing which showed a higher V_{OC} of 0.83 V. As discussed above, the crystallization of PCBM in BHJ could happen only if BHJ layer contact with the crystallized PCBM seed layer during post-annealing. Therefore, the higher V_{OC} can be attributed to the crystallization of PCBM in BHJ layer. It suggests that PCBM crystallites in BHJ layer have smaller EA as observed for the pure PCBM films[9]. Note that V_{OC} of 0.83 V is the highest V_{OC} reported to date for PTB7:PCBM system with BHJ structure. However, the PCE is

lowered because of the decrease of J_{SC} from 10.90 to 6.48 mA cm^{-2} after post-annealing. This could be attributed to unfavorable size of the phase separation or depletion of PCBM in BHJ upon crystallization (see below), which can be potentially solved by optimizing the mixing ratio, use of DIO or a third amorphous acceptor component that remains in the blend layers. Further optimization of the device structures is under investigation. Based on this very first demonstration of using the crystalline PCBM as the acceptor in BHJ device, we believe that it has a potential to exceed the limitation of PCE for PCBM-based OSCs, since V_{OC} could become higher by ~0.1 eV with the same material combinations.

Table 1. The performances of the OSC devices based on PTB7:PCBM BHJ with the various conditions.

Active layer	PCBM seed layer	Post-annealing	V_{OC} (V)	J_{SC} (mA cm^{-2})	FF	PCE (%)
Spin coated	None	None	0.75±0.01	11.81±0.71	0.30±0.03	2.65±0.28
Spin coated	None	150°C	0.76±0.01	10.73±0.69	0.33±0.05	2.69±0.16
Transferred	Amorphous	None	0.75±0.01	11.21±0.91	0.33±0.02	2.77±0.26
Transferred	Amorphous	150°C	0.75±0.01	10.20±0.28	0.30±0.03	2.29±0.23
Transferred	Crystallized	None	0.75±0.01	10.90±1.12	0.33±0.02	2.66±0.29
Transferred	Crystallized	150°C	0.83±0.01	6.48±0.76	0.31±0.06	1.64±0.18

To observe the growth of PCBM crystal in PTB7:PCBM films directly, cross-sectional SEM was performed on the PTB7:PCBM//pre-annealed PCBM/glass samples. Figure 4a shows that without post-annealing, the cross-sectional image showed the presence of a 40-nm-thick pure PCBM layer and a ≥300-nm-thick PTB7:PCBM layer. After post-annealing of the film, the SEM image showed the growth of the PCBM layer to a thickness of approximately 100 nm, whereas the

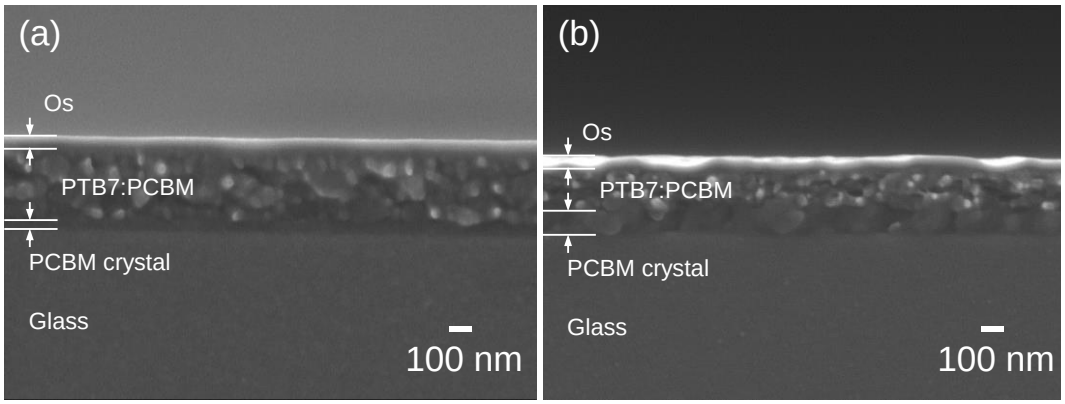

Figure 4. Cross-sectional SEM images of (a) PTB7:PCBM//pre-annealed PCBM and (b) PTB7:PCBM//pre-annealed PCBM after post-annealing. Os layers were deposited on top for protection.

thickness of the BHJ layer was reduced to 180 nm (Figure4b). This suggested that PCBM in the BHJ layer crystallized from the bottom interface and obscured the original interface. The reduced thickness of the PTB7:PCBM layer might be caused by depletion of PCBM from the mixed film and densification by the crystallization of PTB7, as suggested by the XRD results.

The crystallization of PCBM in the BHJ layer from the bottom interface may

indicate the segregation of PTB7 toward the top of the films. To confirm such possibility, incident angle-dependent GIXRD measurements were taken for PTB7:PCBM//pre-annealed PCBM samples. As the X-ray incident angle was reduced, the peak intensity gradually decreased due to the shallower penetration depth of the X-rays (Figure S9). The relative intensity of the peaks from PTB7 and PCBM was calculated from the peak area and plotted as a function of the incident angles (FiguresS9c and d). Before post-annealing, the PCBM and PTB7 peaks (19.5° and 5°, respectively) decreased as the incident angle decreased. After post-annealing, the peak from PTB7 at 5° showed a much smaller dependence on the angles compared with those of crystalline PCBM (10.5° and 17.6°). These results indicated that PCBM segregated to the bottom interface in the BHJ layer during crystallization, and PTB7 segregated to the top of the film, creating a vertical gradient of the components in the BHJ film.

To check the generality of this induced PCBM crystallization in blend films, polymers with different properties, PS (amorphous) and P3HT (highly crystalline) were used instead of PTB7 (Figure 1). The 2DGIXRD results indicated that PCBM crystallized in the PS:PCBM and P3HT:PCBM samples after post-annealing only when the film was in direct contact with the pre-annealed and crystallized PCBM layer (Figure S10). The 2DGIXRD data for the films before and after post-annealing showed similar PCBM diffractions to the PTB7:PCBM case, suggesting the formation of crystallites with the same crystal structure. These results suggest that the

interface-induced crystallization of PCBM can occur in blend films with both amorphous and crystalline polymers, and that it could be a general phenomenon for various types of polymers. However, there are some differences in the intensity and broadness of each spot, which could suggest differences in the sizes, lattice constants, and orientations of the PCBM crystallites. Because the crystallization of PCBM in mixed films should be governed by diffusion in the polymers, the flexibility of the polymer chain could affect the crystallization strongly. A systematic study of the relationship between the glass transition temperature and the crystal structure is necessary to elucidate the crystal structures in detail.

To obtain direct images of the crystallized PCBM domains in the blend films, PS was selectively removed from PS:PCBM//pre-annealed PCBM films after post-annealing by washing with acetone, which is a poor solvent for PCBM but a good solvent for PS. GIXRD patterns before and after washing showed that intensity of the crystalline peaks from PCBM were similar and only the amorphous halo of PCBM decreased substantially (Figure S11). This result suggests that the crystallization happened from the bottom interface, and most of the PCBM in the blend film remained on the surface after washing. A top-view SEM image of the washed film was taken (bird's-eye-view images are also provided in Figure S12). As shown in Figure 5, nanorod-like PCBM structures were observed. The shape and length of the nanorods depended on the PCBM:PS mixing ratios in the films. As shown in Figure 5a, nanorods approximately 150-nm-long were observed when the

PCBM ratio was low (PCBM:PS=0.5:1 by weight). As the PCBM loading increased, the average length of the nanorods increased to 300 nm (PCBM:PS=1:1 by weight) and 500 nm (PCBM:PS=1.5:1 by weight) (Figures 5b and c, respectively). This could be caused by the preferential growth of the PCBM crystals along the long axis of the nanorods, as also suggested by the XRD results. More PCBM in the blend film could increase the supply of PCBM molecules to the interface, increasing the size of the crystallites. SEM images show that the nanorod-like PCBM structure does not have a strong preferred orientation to the thickness direction. This observation might suggest that the pre-annealed PCBM films have a surface consisting of crystallites with random 2D orientation of the growth surface. Because the 2D GIXRD patterns did not change after washing away the PS, the structure observed by SEM should be similar to that in the blend films of PS:PCBM before washing (Figure S10e). UV-vis absorption spectra of the films also remained similar before and after washing (Figure S13). This indicates that almost all the PCBM in PS:PCBM remained on the surface as crystallites.

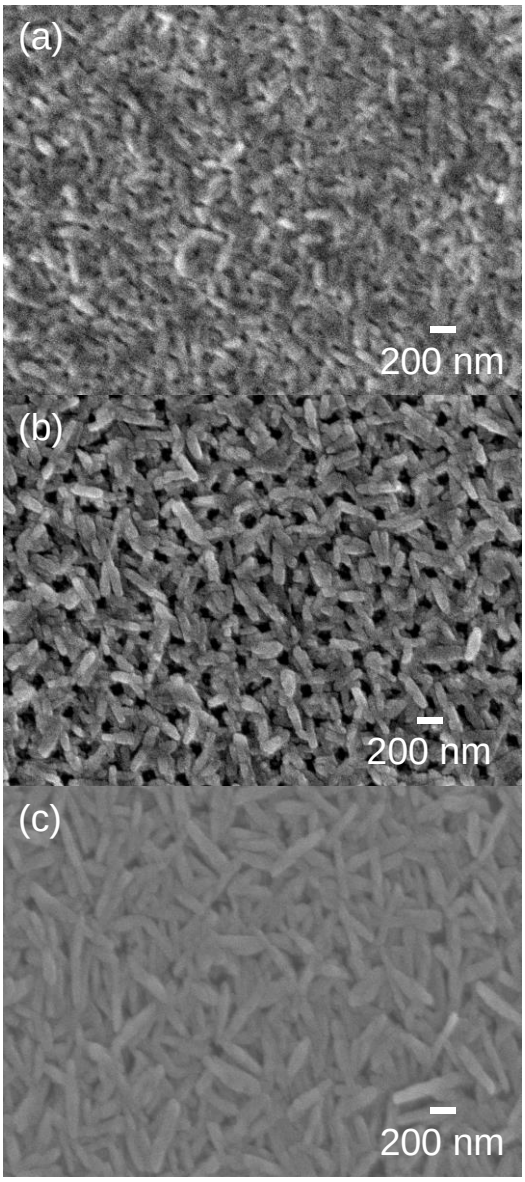

Figure 5. Top-view SEM images of PS:PCBM//pre-annealed PCBM films with PCBM:PS mixing ratios of (a) 0.5:1, (b) 1:1, and (c) 1.5:1 by weight after post-annealing and washing with acetone.

Assuming that epitaxial crystal growth of PCBM occurred in the BHJ from the surface of the crystallized PCBM, the crystal face exposed to the interface could strongly affect the growth and orientation of the crystals. [6,6]-Phenyl-C_{61}-butyric

acid n-butyl ester (PCBNB) is structurally similar to PCBM but has a longer aliphatic tail (butyl vs. methyl, see the chemical structure in Figure S14). PCBNB has high crystallinity with hexagonal packing in thin films after annealing.[30] We used a pre-annealed PCBNB film as the seed layer for PCBM blend films to observe the effects of the surface structure on the crystallization behavior. 2DGIXRD measurements showed that a pre-annealed PCBNB layer also induced the crystallization of PCBM in the PTB7:PCBM layer, although the diffraction patterns were completely different from those of PTB7:PCBM//pre-annealed PCBM after post annealing (Figure S14). Furthermore, optical microscopy showed that large hexagonal crystals of PCBM formed with sizes greater than 100 μm (Figure S16). This striking dependence of the crystallization behavior of PCBM on the seed layer indicated the importance of the structures and the orientations of the crystallites in the seed layers in the induced crystallization.

Conclusion

In this study, we proposed a novel approach to control the crystallization of PCBM in the blend films with various polymers. The nanorod-like PCBM crystalline domain was obtained via interface-induced crystallization. This phenomenon occurred with various polymers and conditions such as film thickness. In contrast, the crystallization was sensitive to the crystal structure of the seed layer, implying that control of the orientation, crystal phase, and crystallite size are possible in a similar way to seed

crystallization in the solution phase or epitaxial growth in vapor deposition. This structure control method could offer an alternative for tuning the morphology of BHJ layers and constructing electron transport pathways with nanorods.[31, 32] The preliminary results on OSCs showed that the crystallization of PCBM in BHJ layer led to the higher V_{OC}, which could push the envelope of the PCBM-based system.

We close our discussions by pointing out that the crystallized nanostructures of PCBM could be also useful as an electron transport layer (ETL) in perovskite solar cells.[33, 34] Preliminarily results show that higher PCE and stability were achieved with the nanostructured PCBM compared to the conventional ETLs like compact TiO_2 or mesoporous TiO_2 (manuscript to be submitted). We believe that deeper understanding of such crystalline phase of the fullerene derivatives could boost the performance of various photovoltaics to the next higher level.

Acknowledgements: This research was supported by JST, PRESTO. Y.F.Z thanks the Chinese Scholarship Council for financial support. The authors thank Ms. Tomoka Kikitsu (RIKEN CEMS) for SAED measurements. GIXRD experiments were performed at beamline BL19B2 and BL46XU of SPring-8 with the approval of the Japan Synchrotron Radiation Research Institute (JASRI) (Proposal 2013B1719 and 2015A1696).

Supporting Information Available: Experimental details, XRD patterns, AFM and

optical microscopy images, SAED patterns, SEM images and absorption spectra of the films. This material is available free of charge via the Internet at http://pubs.acs.org.

References

1. G. Li, V. Shrotriya, J. Huang, Y. Yao, T. Moriarty, K. Emery and Y. Yang, *Nature Materials*, 2005, **4**, 864-868.
2. C. Park, J. E. Park and H. C. Choi, *Accounts of chemical research*, 2014, **47**, 2353-2364.
3. H. Minemawari, T. Yamada, H. Matsui, J. Tsutsumi, S. Haas, R. Chiba, R. Kumai and T. Hasegawa, *Nature*, 2011, **475**, 364-367.
4. N. Stingelin-Stutzmann, E. Smits, H. Wondergem, C. Tanase, P. Blom, P. Smith and D. de Leeuw, *Nat Mater*, 2005, **4**, 601-606.
5. Y. Huang, E. J. Kramer, A. J. Heeger and G. C. Bazan, *Chemical reviews*, 2014, **114**, 7006-7043.
6. G. Paternò, A. J. Warren, J. Spencer, G. Evans, V. G. Sakai, J. Blumberger and F. Cacialli, *Journal of Materials Chemistry C*, 2013, **1**, 5619.
7. M. Casalegno, S. Zanardi, F. Frigerio, R. Po, C. Carbonera, G. Marra, T. Nicolini, G. Raos and S. V. Meille, *Chemical communications*, 2013, **49**, 4525-4527.
8. E. Verploegen, R. Mondal, C. J. Bettinger, S. Sok, M. F. Toney and Z. Bao, *Adv. Funct. Mater.*, 2010, **20**, 3519-3529.
9. Y. Zhong, S. Izawa, K. Hashimoto, K. Tajima, T. Koganezawa and H. Yoshida, *The Journal of Physical Chemistry C*, 2015, **119**, 23-28.
10. S. Gelinas, A. Rao, A. Kumar, S. L. Smith, A. W. Chin, J. Clark, T. S. van der Poll, G. C. Bazan and R. H. Friend, *Science*, 2014, **343**, 512-516.
11. F. C. Jamieson, E. B. Domingo, T. McCarthy-Ward, M. Heeney, N. Stingelin and J. R. Durrant, *Chemical Science*, 2012, **3**, 485-492.
12. A. R. Artem A. B, Vlad G. P, Paul H. M. van Loosdrecht, Maxim S. P, Dorota. N, Jérôme. C, David. B, Richard H. F., *Science*, 2012, **335**, 1340-1344.
13. S. Izawa, K. Nakano, K. Suzuki, K. Hashimoto and K. Tajima, *Adv. Mater.*, 2015, **27**, 3025-3031.
14. C. Groves, *Energy Environ. Sci.*, 2013, **6**, 1546-1551.
15. S. Sweetnam, K. R. Graham, G. O. Ngongang Ndjawa, T. Heumuller, J. A. Bartelt, T. M. Burke, W. Li, W. You, A. Amassian and M. D. McGehee, *J Am Chem Soc*, 2014, **136**, 14078-14088.
16. M. L. Jones, R. Dyer, N. Clarke and C. Groves, *Physical chemistry chemical physics : PCCP*, 2014, **16**, 20310-20320.

17. F. Piersimoni, S. Chambon, K. Vandewal, R. Mens, T. Boonen, A. Gadisa, M. Izquierdo, S. Filippone, B. Ruttens, J. D'Haen, N. Martin, L. Lutsen, D. Vanderzande, P. Adriaensens and J. V. Manca, *J. Phys. Chem. C*, 2011, **115**, 10873-10880.
18. M. Campoy-Quiles, T. Ferenczi, T. Agostinelli, P. G. Etchegoin, Y. Kim, T. D. Anthopoulos, P. N. Stavrinou, D. D. Bradley and J. Nelson, *Nat Mater*, 2008, **7**, 158-164.
19. Y. Sun, G. C. Welch, W. L. Leong, C. J. Takacs, G. C. Bazan and A. J. Heeger, *Nat Mater*, 2012, **11**, 44-48.
20. M. Y. Chiu, U. S. Jeng, C. H. Su, K. S. Liang and K. H. Wei, *Advanced Materials*, 2008, **20**, 2573-2578.
21. D. Mon, A. M. Higgins, D. James, M. Hampton, J. E. Macdonald, M. B. Ward, P. Gutfreund, S. Lilliu and J. Rawle, *Physical chemistry chemical physics : PCCP*, 2015, **17**, 2216-2227.
22. A. Swinnen, I. Haeldermans, M. vande Ven, J. D'Haen, G. Vanhoyland, S. Aresu, M. D'Olieslaeger and J. Manca, *Advanced Functional Materials*, 2006, **16**, 760-765.
23. J. J. Richards, A. H. Rice, R. D. Nelson, F. S. Kim, S. A. Jenekhe, C. K. Luscombe and D. C. Pozzo, *Advanced Functional Materials*, 2013, **23**, 514-522.
24. K. T. Shoji Miyanishi, and Kazuhito Hashimoto, *Macromolecules* 2009, **42**, 1610-1618.
25. C. Lindqvist, J. Bergqvist, C.-C. Feng, S. Gustafsson, O. Bäcke, N. D. Treat, C. Bounioux, P. Henriksson, R. Kroon, E. Wang, A. Sanz-Velasco, P. M. Kristiansen, N. Stingelin, E. Olsson, O. Inganäs, M. R. Andersson and C. Müller, *Advanced Energy Materials*, 2014, **4**, 1301437.
26. L. Zheng, J. Liu and Y. Han, *Phys. Chem. Chem. Phys.*, 2013, **15**, 1208-1215.
27. Q. Wei, S. Miyanishi, K. Tajima and K. Hashimoto, *ACS Appl. Mater. Interfaces*, 2009, **1**, 2660-2666.
28. Q. Wei, K. Tajima and K. Hashimoto, *ACS Appl. Mater. Interfaces*, 2009, **1**, 1865-1868.
29. L. Lu and L. Yu, *Adv Mater*, 2014, **26**, 4413-4430.
30. S. H. Choi, C. D. Liman, S. Kramer, M. L. Chabinyc and E. J. Kramer, *The journal of physical chemistry. B*, 2012, **116**, 13568-13574.
31. K. Takanezawa, K. Tajima and K. Hashimoto, *Appl. Phys. Lett.*, 2008, **93**.
32. K. Takanezawa, K. Hirota, Q.-S. Wei, K. Tajima and K. Hashimoto, *J. Phys. Chem. C*, 2007, **111**, 7218-7223.
33. K. Wojciechowski, T. Leijtens, S. Siprova, C. Schlueter, M. T. Horantner, J. T. Wang, C. Z. Li, A. K. Jen, T. L. Lee and H. J. Snaith, *The journal of physical chemistry letters*, 2015, **6**, 2399-2405.
34. Y. Shao, Z. Xiao, C. Bi, Y. Yuan and J. Huang, *Nature communications*, 2014, **5**, 5784.

TOC graphic

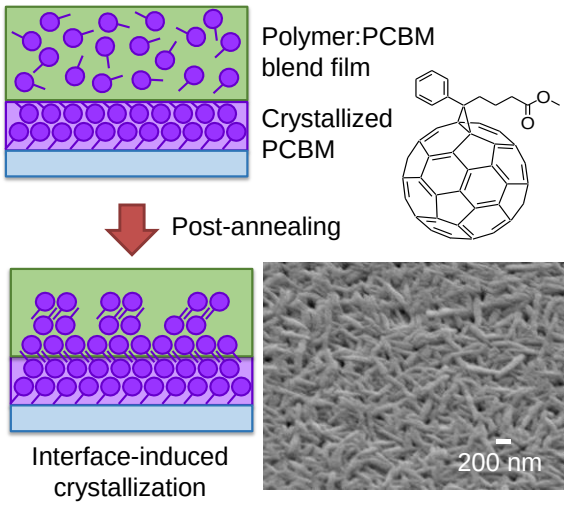
Polymer:PCBM
blend film
Crystallized
PCBM
O
O
Post-annealing
Interface-induced
crystallization
200 nm